ARTICLE

Check for updates

US Gulf Coast tropical cyclone precipitation influenced by volcanism and the North Atlantic subtropical high

Joshua C. Bregy [1,2✉], Justin T. Maxwell [1], Scott M. Robeson [1], Grant L. Harley [3], Emily A. Elliott [4] & Karen J. Heeter [3]

Understanding the response of tropical cyclone precipitation to ongoing climate change is essential to determine associated flood risk. However, instrumental records are short-term and fail to capture the full range of variability in seasonal totals of precipitation from tropical cyclones. Here we present a 473-year-long tree-ring proxy record comprised of longleaf pine from excavated coffins, a historical house, remnant stumps, and living trees in southern Mississippi, USA. We use cross-dating dendrochronological analyses calibrated with instrumental records to reconstruct tropical cyclone precipitation stretching back to 1540 CE. We compare this record to potential climatic controls of interannual and multidecadal tropical cyclone precipitation variability along the Gulf Coast. We find that tropical cyclone precipitation declined significantly in the two years following large Northern Hemisphere volcanic eruptions and is influenced by the behavior of the North Atlantic subtropical high-pressure system. Additionally, we suggest that tropical cyclone precipitation variability is significantly, albeit weakly, related to Atlantic multidecadal variability. Finally, we suggest that we need to establish a network for reconstructing precipitation from tropical cyclones in the Southeast USA if we want to capture regional tropical cyclone behavior and associated flood risks.

[1] Department of Geography, Indiana University, Bloomington, IN, USA. [2] Department of Earth and Atmospheric Sciences, Indiana University, Bloomington, IN, USA. [3] Department of Earth and Spatial Sciences, University of Idaho, Moscow, ID, USA. [4] Department of Geography, University of Alabama, Tuscaloosa, AL, USA. ✉email: jbregy@indiana.edu

The devastation brought about by storm surge and high winds from tropical cyclones (TCs) can reshape coastlines and communities alike. Tropical cyclone precipitation (TCP), however, is an often-overlooked hazard, despite inland flooding from TCP being the leading cause of TC-related fatalities[1] and resulting in extensive damage to natural and built environments. TCP can trigger additional cascading hazards such as slope failure[2], eutrophication[3], and outbreaks of waterborne pathogens[4]. Conversely, TCP is an important element of regional hydroclimates[5] that influences critical water management decisions[6], maintains essential ecosystem services and functions[7], and provides much-needed relief from droughts[8]. Climate models indicate that TC precipitation rates are projected to increase due to reduced storm translation speeds[9], warming sea surface temperatures (SSTs), and increased vapor pressure[10] in response to anthropogenic warming. The importance of TCP and its anticipated changes in response to greenhouse forcing warrant further exploration of the full range of variability in TCP quantities.

Precipitation and TC variability along the Gulf Coast are driven, in part, by several climatic features of the North Atlantic basin, such as the North Atlantic subtropical high[5,11–13], the North Atlantic Oscillation[13,14], and multidecadal sea-surface temperature variability in the North Atlantic[13,15]. However, our understanding of these mechanisms is based on short instrumental records, some of which do not capture a complete cycle of the ascribed climatic controls. Developing longer records of TCs from paleoclimate proxies can provide additional context to help understand the response of TCs to greenhouse forcing by sampling longer variations in TC activity, intensity, and hazards. Attribution studies suggest that climate change is a threat multiplier that exacerbates the effects of a TC, such as the excessive TCP totals from Hurricane Harvey (2017)[16]. Nevertheless, linking changes in TC behavior to the complex effects of anthropogenic climate change is complicated by limited instrumental records[17] (HURDAT2: 1850–present[18]; TCPDat: 1948–present[5]), necessitating records extending beyond the observational period. Sediment deposits formed by storm surge are arguably the most frequently employed proxy for paleohurricane reconstruction[19,20]. Overwash and other sediment deposits can provide centennial- to millennial-length records of TC frequency and storm characteristics[21–24], including wind speed[22,24] and storm surge height[19,23]. However, only the most intense storms tend to leave signatures as many of these records are in lacustrine or back-barrier environments and are heavily dependent on coastal geomorphology, hydrodynamic conditions, and storm characteristics[19]. Therefore, the temporal consistency afforded by high-resolution records are critical to supplement event gaps for coarser records[25–28].

Annual-resolution TC reconstructions are less common than sediment-based proxies, and typically come from isotopic ratios measured in speleothems[29] or tree rings[30]. These proxies typically reconstruct TC activity (e.g., presence/absence) rather than TCP, and presently only three studies have used tree-ring-width derived metrics to produce TCP estimates[31–33]. The three studies reconstructed TCP estimates since the 1700s using longleaf pine in the coastal plains of North and South Carolina, USA. Here, we focus on reconstructing TCP along the Mississippi Gulf Coast, an area affected by an average of ~1 TC year^{-1} based on instrumental records[18] (Fig. 1). Although several studies have reconstructed pre-industrial extreme TC variability along the Gulf Coast[20], centennial-scale reconstructions of TCP variability in the region are nonexistent. Here, we present a record of July–September TCP totals spanning 1540 to 2012 CE, representing the longest annual TCP reconstruction to date, and the first TCP reconstruction for the Gulf Coast, USA. We use our 473-year record to (1) examine multidecadal patterns in Gulf Coast TCP and (2) identify potential climate controls of TCP over

varying spatiotemporal scales. We find that over interannual timescales, major Northern Hemisphere eruptions as well as the North Atlantic subtropical high are important influences on TCP along the north-central Gulf Coast. Additionally, over multidecadal intervals, TCP in the study area exhibits a significant, albeit weak, correlation with changes in Atlantic multidecadal variability (AMV).

Results and discussion

TCP reconstruction. We collected samples from longleaf pine (*Pinus palustris*, Mill.; hereinafter longleaf) trees in the De Soto National Forest (DNF) in Mississippi, which is a humid subtropical climate (Supplementary Fig. 1) that receives abundant TCP (25–45 mm year^{-1}; Fig. 1)[5]. Unfortunately, Euro-American land-use practices (e.g., widespread logging, naval stores industry) led to a 98% reduction in longleaf range since the early 1800s[34], severely limiting the modern availability of old longleaf records from forests in the region. To overcome this, in addition to sampling living and remnant-logged stumps, we utilized cores of archeological specimens from coffins from recently excavated burial sites[35] and historical structures[36] to produce the 473-year tree-ring chronology from which our TCP reconstruction was developed (Fig. 1b and Supplementary Fig. 2; see "Methods"). Adjusted latewood ring width (LWa; Supplementary Fig. 3; see "Methods") at the series level showed the strongest correlation with TCP ($r = 0.60–0.64$; $p < 0.05$; Fig. 2a and Supplementary Fig. 4), and we therefore used LWa as the predictor in a linear regression reconstruction model. Our reconstruction model captures 40% of the variance in instrumental TCP (Fig. 2a, b and Supplementary Table 1) and is temporally stable (Supplementary Table 2). Series-level LWa had a substantially lower correlation with non-TC precipitation ($r = 0.30–0.40$; $p < 0.05$) than TCP (Supplementary Fig. 4), suggesting that longleaf in the Gulf Coast region are sensitive to the short duration, high volume input of water that TCP typically provides, like the longleaf forests in North and South Carolina[31–33]. This sensitivity to TCP likely arises from the combination of high rainfall rates characteristic of TCs[37], gently varying topography[38,39], and xeric, sandy soils with high infiltration rates[38–40] that allow large volumes of rainwater to quickly reach and raise the water table depth, thereby granting the shallow lateral roots of longleaf pine access to water that was previously only accessible to the central taproot[41]. We limited our period of coverage to 1540–2012 CE (Fig. 2c) due to a decreased sample size prior to 1540. While LWa slightly overestimates TCP whenever LWa and instrumental TCP totals are low (Fig. 2a, b), it generally tracks TCP variability well.

Since 1540 CE, there are 19 years during which TCP totals exceed 100 mm (96th percentile), five of which surpass 157 mm (99th percentile): 1569, 1749, 1888, 2005, and 2012 CE (Fig. 2c). In certain cases, we can attribute these outliers to multiple TCs, such as during 2005, or to specific events, such as the 1888 Louisiana hurricane and Hurricane Isaac (2012), demonstrating that individual storms can potentially produce rainfall totals comparable to seasonal totals from multiple storms. Overall, the annually resolved record is not autocorrelated (Supplementary Fig. 5), indicating that TCP totals are not persistent from year to year. However, analyzing the time series with moving windows captures some low-frequency behavior of TCP, specifically over multidecadal timescales (Fig. 2c, d). At this scale, there are distinct periods of low (e.g., 1620–1660 CE) and high (e.g., 1860–1890 CE) 10-year-mean TCP totals relative to the reconstruction mean (28.8 mm year^{-1}; Fig. 2c, d).

We calculated the frequency of years experiencing TCP totals in the fourth quartile (Q4), which is 42.2 mm year^{-1} for our study area (Fig. 2d) using a 50-year moving sum to understand
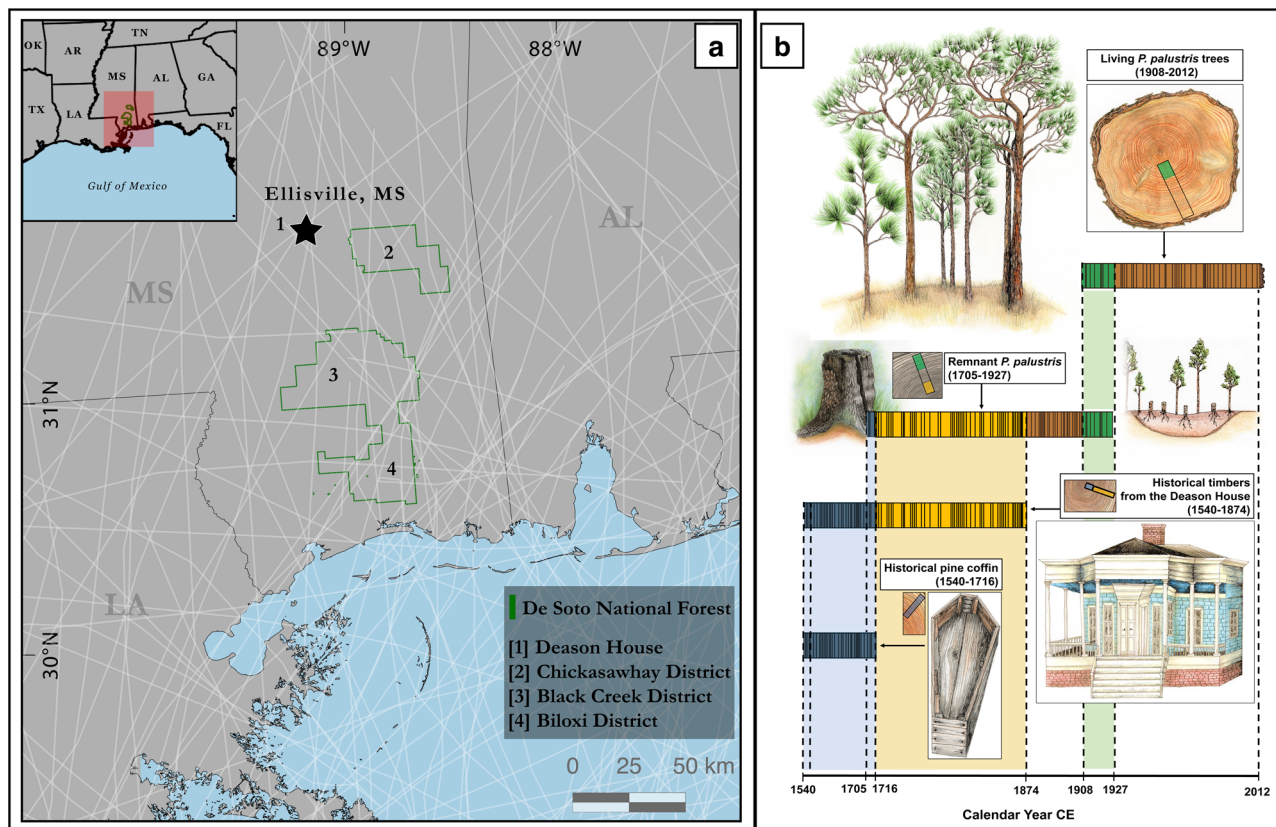
Fig. 1 Tropical cyclone tracks at De Soto National Forest and cross-dating techniques. a Tracks (white lines) of all tropical cyclones (tropical depressions, tropical storms, and hurricanes) within 223 km of the De Soto National Forest, Mississippi (dark green) from 1850 to present. Using instrumental records, the Mississippi Gulf Coast is a humid subtropical environment (Supplementary Fig. 1) that experiences ~1 TC per year[13] and receives an average of 25–45 mm year^{-1} of TCP[5]. However, this region has had multiple direct landfalls from catastrophic hurricanes over the past 2500 years based on overwash deposits[23]. The plotted storm track data are from HURDAT2[18]. **b** Diagram demonstrating the principle of cross-dating. By incorporating wood from stumps, coffins[31], and the Deason Home in Ellisville, Mississippi[32], we were able to extend our reconstruction to the 1500s.

multidecadal patterns in the frequency and timing of extreme TCP. Like the patterns seen in multidecadal TCP totals (Fig. 2d), low-frequency behavior occurs in the frequency of Q4 years, with periods above and below the mean frequency (12.2 years) defined as wet and dry TCP intervals, respectively (Fig. 2d). Wet intervals occur during the late 1600s and early 1700s, mid- to late 1800s, and throughout much of the 1900s, with dry periods interspersed between these intervals.

Interannual climate controls. We analyzed seasonal TCP totals and the Bermuda high index (BHI)[42] using Spearman's rank correlation, demonstrating that changes in the western flank of the North Atlantic subtropical high may influence TCP variability during the common period (1948–2012; $\rho = 0.30$; $p < 0.05$; Fig. 3a–c). Western flank variability shifts storm tracks and landfall locations[43], subsequently affecting terrestrial TCP distributions[5]. When the flank is positioned farther west (east) of its mean location, TCP decreases (increases) along the north-central Gulf Coast. Time series for the magnitude of the correlations between reconstructed TCP and the BHI match that of instrumental TCP and the BHI[5] (Fig. 3a–c). TCP and BHI likely exhibit similar interactions prior to the start of the instrumental record; however, given the short instrumental record and the complex dynamics of the hurricane-TCP connection, annually resolved, long-term reconstructions of the BHI are necessary to further evaluate this relationship over longer timescales.

Previous studies have also identified explosive volcanic eruptions as an external forcing mechanism for TCs on interannual timescales[44–47]. For example, following the eruptions of El Chichón (1982) and Pinatubo (1991), TC activity declined in the North Atlantic in response to volcanic aerosol injections[44]. However, it is difficult to determine the degree to which these eruptions affected North Atlantic TCs due to co-occurring El Niño events[44]. Interestingly, Altman et al. (ref. [43]) found that latewood δ^{18}O responded to eruption intensity as measured by the Volcanic Explosivity Index (VEI) rather than stratospheric sulfate aerosol volumes, suggesting that ash volume may also force variations in TC behavior.

To examine the role of short-term external forcing by volcanism, we conducted a superposed epoch analysis between TCP and notable volcanic eruptions (Fig. 3d, e and Supplementary Table 3). For our analysis, we selected tropical volcanoes that were large enough to affect global climate (VEI ≥6; e.g., Tambora—1815)[47,48] or eruptions that were large enough to have at least a regional impact on the climate of the Southeast US and/or Gulf of Mexico (hereinafter Gulf; VEI ≥4; Fig. 3d and Supplementary Table 3). Our superposed epoch analysis results indicate that TCP declines significantly ($p < 0.05$) in the 2 years following an eruption event before returning to near-normal values (Fig. 3e).

While global climate simulations and reconstructions over the last millennium suggest that global mean precipitation decreases following explosive volcanic eruptions[49], regional hydroclimates exhibit substantially more heterogenous shifts in response to volcanic activity[50]. Likewise, instrumental records indicate volcanically induced declines in global precipitation on intra-annual timescales[51]; however, our understanding of how
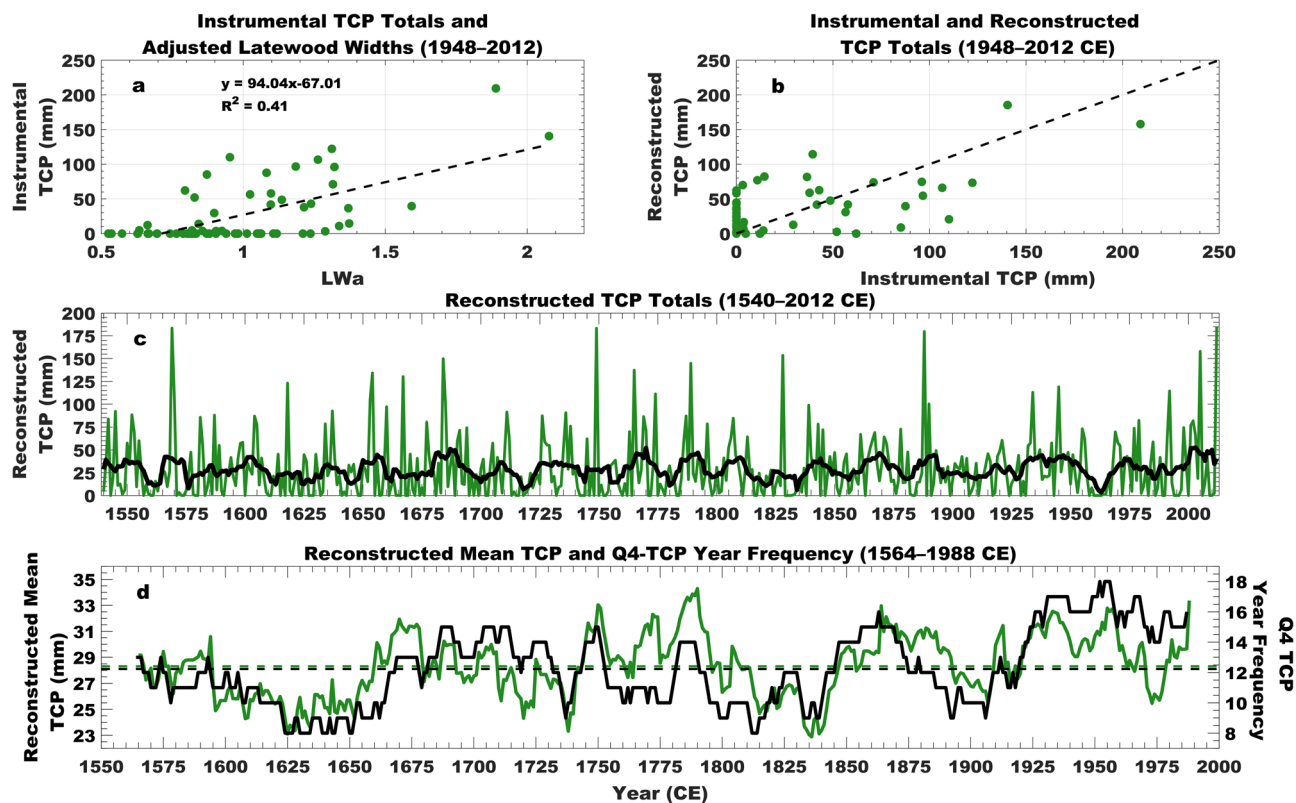
Fig. 2 Reconstruction of tropical cyclone precipitation. a Scatterplot between seasonal (July–September) instrumental TCP totals (mm) and adjusted latewood width (LWa) during the calibration period (1948–2012 CE). Black dashed line is the regression line. LWa and instrumental TCP exhibited a strong significant correlation with one another ($r = 0.64$; $p \ll 0.001$). **b** Same as in **a** but using instrumental and reconstructed TCP totals instead. Black dashed line is the 1-to-1 line. **c** Annually-resolved reconstruction of seasonal TCP totals (green line) and a 10-year running average (black line) for the study period (1540–2012 CE). The peaks in the 10-year running average are an approximate marker of the fourth quartile cutoff (≥ 42.2 mm) used to calculate the frequency curve shown in **d**. **d** Reconstructed 50-year mean seasonal TCP totals (green line) and the frequency years with TCP totals ≥ 42.2 mm (fourth quartile, or Q4; black line) during the study period. A 50-year moving average and 50-year moving window were used to calculate mean TCP and Q4 frequency, respectively. Green and black dashed lines represent the averages of mean TCP (28.8 mm year^{-1}) and Q4 frequency (12.3 events 50-years^{-1}), respectively.

precipitation responds to volcanic eruptions on spatial scales relevant to TCs remains uncertain. Therefore, we suspect that our results indicate a reduction in storm activity rather than TCP per event declining in response to an eruption. This finding is consistent with prior studies documenting reductions in TC activity in the years following large eruption events[44–47].

The timing of changes in TCP in our record is coincident with several major eruption events (Fig. 3d and Supplementary Table 3). For example, the early to mid-1800s is marked by multiple large eruption events, including Tambora (1815 CE), that injected large quantities of ash and sulfate aerosols into the troposphere and stratosphere, respectively, and altering regional and global climate conditions[48]. At the same time, TCP exhibits a decline that may be partially attributable to these eruptions (Fig. 3d). Further, this response is not unique to our record; longleaf records from North Carolina show a period of suppressed tree growth—and by extension, reduced TCP—during the same interval as these eruptions, particularly Tambora[31]. Likewise, declines in TC frequency elsewhere, such as the western North Pacific, have been attributed to volcanic ash[47], which acts as an external radiative forcing mechanism, allowing weaker eruptions (i.e., $4 \leq VEI < 6$) to exert an influence on regional climates[52].

Ash clouds induce surficial cooling directly by reducing insolation[52] that can result in marked declines in TC frequency in the years following an eruption[47]. We suspect that ash plumes from eruptions more proximal to our site (e.g., El Chichón, Mexico) act in a comparable manner as dust plumes originating from the Sahara Desert. Dust outbreaks are known to result in cooler SST anomalies in the North Atlantic Ocean[49], which can reduce TC frequency[53,54]. While volcanic ash plumes are markedly different from dust plumes, they may induce similar changes to radiative forcing driving regional climate variability, including tropical cyclogenesis potential. For smaller, more proximal eruptions, the ejected ash could potentially cool SSTs in the Gulf and Caribbean Sea, reducing the number of TCs that form or make landfall along the north-central Gulf Coast. In either case, the effects of such eruptions can persist in upper oceans for several years[55] in regions of tropical cyclogenesis[44,46]. Thus, externally forced surface cooling reduces the tropical cyclogenesis potential by hindering air-sea heat exchange as well as increasing vertical wind shear via the wind-evaporation-SST feedback[44,46,56].

Multidecadal climate controls. Explosive eruptions from tropical volcanoes that inject sulfate aerosols into the stratosphere are an important external forcing behind multidecadal cooling in the North Atlantic[57–59]. Considering this, we examined our record in the context of an annually-resolved reconstruction of AMV[58] to understand long-term connections between SSTs and TCP (Fig. 4a, b and Supplementary Figs. 6–9). We document a connection between AMV and TCP over multiple timescales (Fig. 4a, b and Supplementary Figs. 7–9). The connection over interannual intervals is weak ($r = 0.11$; $p < 0.05$; Fig. 4b); however, in addition to exhibiting a concurrent connection, the
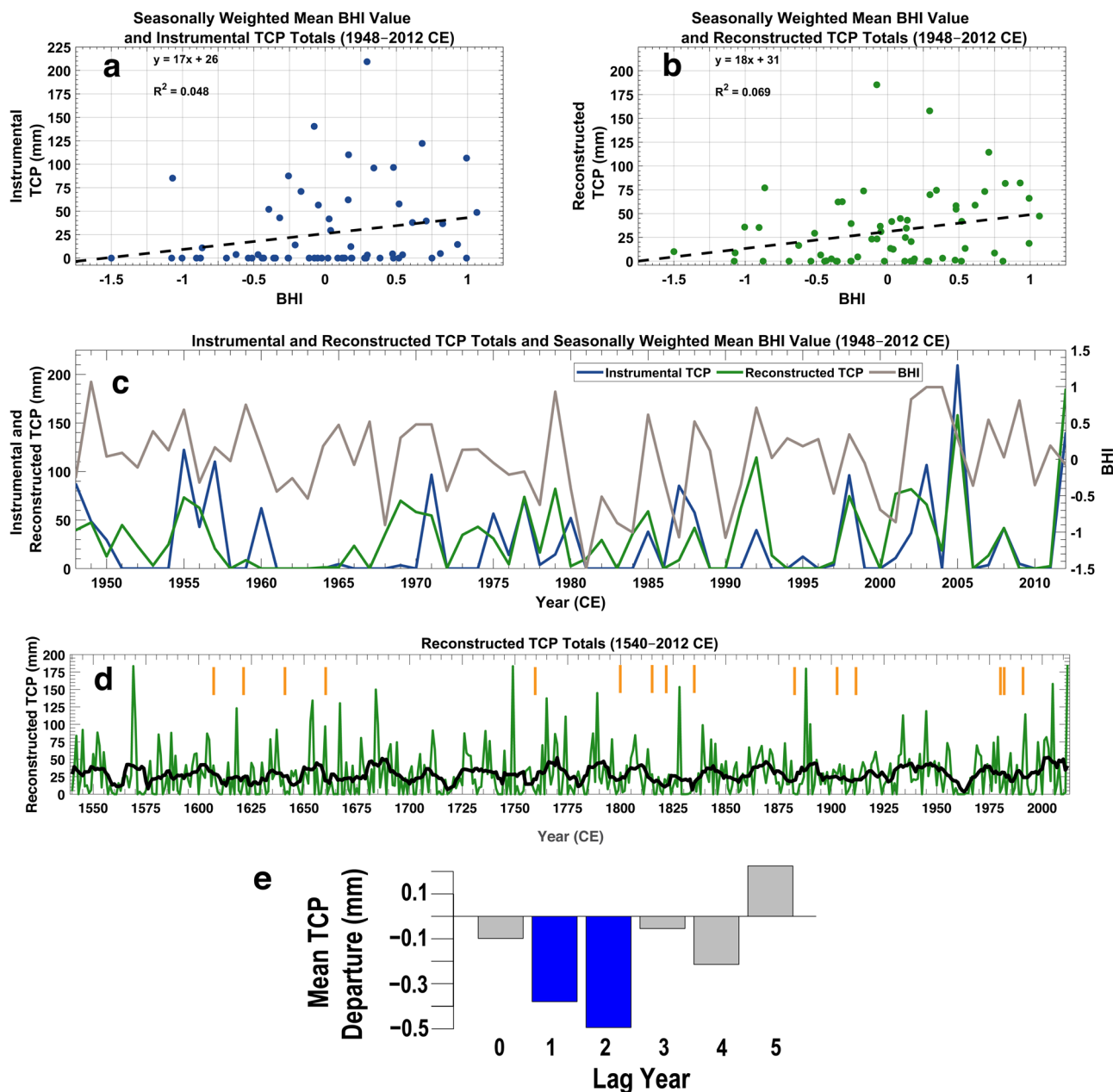
Fig. 3 Interannual climate controls of TCP. a Scatterplot between seasonally weighted mean BHI values and seasonal (July–September) instrumental TCP totals (mm) during the calibration period (1948–2012 CE). Monthly BHI was calculated following Katz et al. (ref. [38]), and the seasonal mean BHI was weighted by the average number of tropical cyclone landfalls per month. Black dashed line is the linear regression model line. **b** Same as in **a** but using the reconstructed seasonal TCP totals instead. **c** Time series of mean BHI (light brown line), instrumental TCP totals (dark blue line), and reconstructed TCP totals (green line) during the calibration period. **d** Annually resolved reconstruction of seasonal TCP totals (green line), a 10-year running average (black line), and volcanic eruptions (orange markers; Supplementary Table 3) for the study period (1540–2012 CE). **e** Superposed epoch analysis between TCP and volcanic eruptions, which were selected following the methods described in Altman et al. (ref. [43]). Analysis extended to 5 years following an eruption, with columns indicating the departure from the mean during lag years 0–5. Blue shading on bars indicates significance ($p < 0.05$).

AMV also leads TCP by several years, a characteristic typical of the relationship between multidecadal SSTs in the North Atlantic and TC activity[60]. Likewise, we see a connection between multidecadal AMV and TCP behavior ($r = 0.56$–0.61; $p < 0.05$; Fig. 4a and Supplementary Figs. 7 and 8), and while smoothing can inflate the relationship between two time series (Supplementary Fig. 6), we still see a connection with similar lag-lead behavior after accounting for autocorrelation (Supplementary Figs. 7, 8B, and 10).

At longer intervals, TCP and AMV seem to be generally in-phase with one another (Fig. 4a and Supplementary Figs. 8A and

9), with periods of anomalously low TCP values correspond to similarly low AMV values (Supplementary Fig. 9). However, there is no consistent phasing between TCP and the AMV over annual to interannual timescales (Supplementary Fig. 10), further reinforcing a complex connection between the two. While SSTs and TCP are tightly coupled[61], the lack of a strong connection between AMV and TCP at our site likely reflects a difference in spatial scale. The AMV represents an integration of SSTs across the entire North Atlantic basin, whereas our reconstruction reflects TCs that tracked ≤223 km from the north-central Gulf Coast. As such, site-level TCP reconstructions, especially those
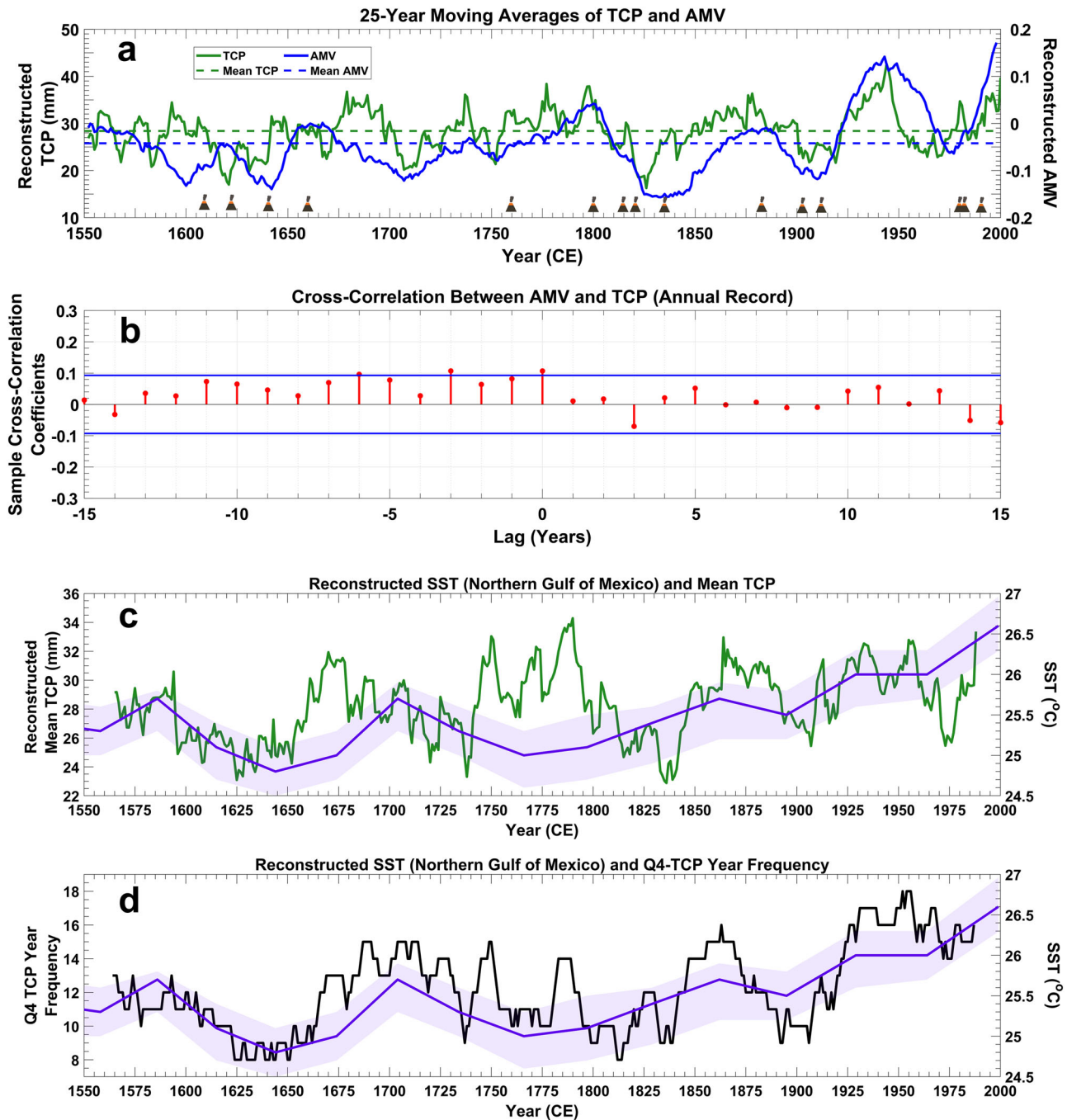
Fig. 4 Multidecadal climate controls of TCP. a Time series of reconstructed tropical cyclone precipitation (TCP; green line) and Atlantic multidecadal variability (AMV; blue line)[53] from 1540 to 2010 using a 25-year moving average. Volcano symbols mark the timing of eruption events included in the superposed epoch analysis (Supplementary Table 3). Green and blue dashed lines are the mean TCP and AMV, respectively. **b** Cross-correlation coefficients (red lines) between detrended annual values of TCP and AMV extending to lag ±15. Blue lines represent the significance threshold, which were corrected for autocorrelation following Cryer and Chan (ref. [92]) and Dean and Dunsmuir (ref. [93]). **c** Time series of reconstructed seasonal (July–September) mean TCP totals (green line; left axis; mm) and the Loop Current as represented by SSTs from the northern Gulf of Mexico (lavender line; right axis; °C)[100]. Mean TCP was calculated using a 50-year moving average. Lavender shading represents the 95% confidence intervals for SSTs. **d** Same as in **a** but using the frequency of years with TCP totals reaching the fourth quartile (≥42.2 mm; Q4; black line; left axis). Q4 frequency was calculated using a 50-year moving sum.

located in semi-enclosed basins, are potentially more sensitive to punctuated events (e.g., volcanoes) or regional drivers of TC variability (e.g., tropical SSTs).

The Atlantic Warm Pool (AWP), which influences environmental favorability for TC formation and intensification by acting as a conduit between TCs and basin-scale SST variability in the

North Atlantic[62,63], could potentially explain the weak, yet significant lagged relationship between the AMV and TCP. The size of the AWP, defined by the area located within the 28.5 °C isotherm, acts in concert with the AMV, with warmer (cooler) phases causing a larger (smaller) AWP[62,63]. Consequently, AWP variability leads to changes in vertical windshear and convective

instability across the tropical Atlantic, including the Caribbean and Gulf[62,63]. A larger AWP produces a more favorable environment for tropical cyclogenesis, while the opposite occurs when the size of the AWP is reduced[62,63]. As the AWP is an important moisture source for summer and autumnal precipitation in the southeastern US[62,63], it serves a similar function regarding the amount of precipitation that TCs produce and is likely an important connection between the AMV and TCP variability along the northern Gulf Coast.

A larger AWP would also include a greater portion of the Gulf, with the Loop Current being an extension of the AWP[64]. The northward migration of the Loop Current into the Gulf reflects an expanding AWP, creating regional-to-local environment conducive for sustaining or augmenting TC intensity and/or wetness. Given the role that the Loop Current plays in controlling the thermal structure of the Gulf[64], we propose that shifts in the mean position of the Loop Current or changes in the frequency of eddy shedding influence TCP activity along the north-central Gulf Coast (Fig. 4c, d). When the Loop Current is displaced farther north into the Gulf, the northern Gulf Coast moves into a wet phase (e.g., ~1675–1725), while the opposite occurs during a relaxed Loop Current (e.g., ~1600–1650; Fig. 4c, d). Previous studies corroborate this relationship, which shows long-term changes in Loop Current position or activity forcing centennial-scale shifts in regional storm activity[22,23]. While our findings indicate that the AMV has a less direct role in driving TCP variability on the Gulf Coast, regional phenomena (i.e., AWP) that influence SST distribution, upper-ocean heat content, vertical wind shear, and latent heat fluxes may act as a direct mechanism behind TCP variability while also linking longer patterns of TCP and the AMV. As such, further illuminating the drivers of TCP over different spatiotemporal scales will require the development of a TCP reconstruction network and incorporating modeled oceanographic and atmospheric patterns over the last millennium (e.g., Last Millennium Reanalysis[65–67]).

Conclusions

Our annually resolved 473-year record of TCP allows us to further characterize drivers of TC variability over multiple timescales. Records such as ours and those from the Carolinas[31–33] enable us to understand pre-industrial TC variability from a unique dimension. Not only does our record provide insight into the drivers of TCP variability as well as the occurrence of extreme events, but it also demonstrates that longleaf pine elsewhere in the southeastern US could potentially contain similarly long records of TCP. Given the spatial footprint of climate signals that tree-ring records can afford, it is critical that future research efforts focus on developing a network of TCP reconstructions that complements existing paleohurricane records to characterize regional TC-climates. Extending record lengths and developing such a network of long-term TCP reconstructions will require incorporating unique longleaf pine wood sources (e.g., coffins, historical houses) into chronologies, or investigating the efficacy of using LWa of other southern pine species in the Southeast to reconstruct TCP. Given the worldwide export of longleaf pine timber resulting from widespread European and American harvesting practices, international institutes and archives may house wood samples and essential records (e.g., receipts) about wood sources, and may therefore be an invaluable resource for building an extensive network of long-term TCP reconstructions[68].

Another benefit of our reconstruction is that we can begin making multi-century connections to past TC-related flood events. Linking historical flooding, especially in smaller watersheds, to TCs is critical to discerning flood frequencies and large-scale watershed hydrodynamics in response to changes in the hurricane-climate

system. For example, heightened flood probabilities throughout the southeastern US occurred during the Little Ice Age, reaching a maximum likelihood toward the end of the anomalously cool period[69]. Whether this increased probability stems from changes in the TC hydroclimate remains uncertain. However, considering that the probability of high-magnitude flooding (e.g., 100-year return interval) can be exacerbated by fluvial engineering practices (e.g., channel straightening)[70], identifying these connections can help to determine the underlying climatic drivers of flooding in hurricane-prone regions. While widespread TC-induced flooding along major rivers like the Mississippi River is rare, smaller drainage basins often flood from extreme precipitation events like TCs. The expected changes to the TC climate—including the length of hurricane season and TCP extremes—in response to climate change increases the number of days with TCP-flood risks by 28–180% in the southeastern US[71]. Reconstructions such as ours provide the context needed in determining annual to multidecadal flood risks and hydrologic variability across a range of spatial scales. Incorporating such reconstructions into proxy-enabled models is critical to understanding the climatic setting of hydrologic variability, reducing hazard risk and exposure in vulnerable coastal communities.

Materials and methods

Field methods. We sampled longleaf pine (*Pinus palustris* Mill.; hereinafter longleaf) within the DNF in Mississippi between 2012 and 2013 (Fig. 1a). Longleaf radial growth variability is controlled predominantly by stochastic extreme precipitation events (e.g., TCs)[72]. Unlike previous studies that sampled trees atop the sandy ridges of Carolina bays[31–33,41], we sampled trees with old-growth characteristics[73] across multiple microhabitats in the longleaf pine forests of south Mississippi. Following the methods of Stokes and Smiley[74], we collected at least two samples from opposite sides of each living tree at ~1.5 m. We also collected cross-sections from remnant stumps in DNF using a chainsaw. To extend our chronology back in time (Fig. 1b and Supplementary Fig. 2), we leveraged archeological wood samples from the Deason Home (Ellisville, MS)[36] and wooden coffins (Mississippi State Asylum Cemetery)[35], both of which were constructed using longleaf pine sourced from DNF based on historical lumber receipts[32]. Although written and oral records of the house have produced unreliable construction dates, Harley et al.[36] used annual growth rings and tree-ring-derived cutting dates to cross-date with the De Soto reference chronology to identify the years of three major construction sequences, including the initial construction of the house during the winter of 1835/1836. The wooden coffins were also cross-dated with the reference chronology and Deason Home using annual growth measurements. As these samples were initially cross-dated using annual ring widths, we remeasured these samples, in addition to previously unmeasured samples, to collect early- and latewood widths and extend the DNF chronology back in time.

Laboratory methods. We prepared samples for analysis following standard dendrochronological techniques[75]. We mounted cores and cross-sections for stability while sanding samples with progressively finer sandpaper (to 600 ANSI) to reveal ring structure[74–77]. Next, we visually cross-dated and scanned samples using WinDendro (v. 2017a). Although latewood width was our primary interest because it exhibits the greatest hydrologically driven variations in width[72], we also measured earlywood width to calculate the adjusted latewood width index (see the following section). Next, we used the program COFECHA[78] to statistically confirm visual cross-dating of the samples, starting with cores from living trees (most recent year: 2012). For cross-sections, we measured ring widths along two transects radiating from the innermost rings, along which we measured early-, latewood, and total ring width using WinDendro (v. 2017a). To date the unanchored transects, we used COFECHA to statistically correlate ring-width measurements from transects with those from the dated, living trees (Fig. 1b). Although many samples were previously cross-dated for other studies[36,79], we expanded the chronology by including previously undated samples from living trees, stumps, the Deason Home, and coffins, increasing our sample depth and extending our chronology back to the early sixteenth century (Fig. 1b and Supplementary Fig. 2). After cross-dating all the samples, we detrended each series using ARSTAN[80] to fit a two-thirds smoothing spline[81], with the recommended adjustment[82], to remove as much biological and non-climatic growth from our early- and latewood measurements.

Adjusted latewood width. In many *Pinus* species, latewood growth can be affected by climate conditions during earlier portions of the growing season[83–85]. However, accounting for growth related to antecedent climate conditions can strengthen the relationship between latewood production and the associated climate controls. This method is frequently used in monsoon reconstructions in the southwestern US where previous pluvials or droughts can dampen the monsoon signal preserved in latewood, especially when monsoon precipitation is near or below normal[83–85].

Knapp et al.[31] found that the timing of latewood growth coincides with the occurrence of the majority of TCP, and as such, latewood width can be used to reconstruct estimations of seasonal TCP totals[32,33]. Given that the Southeast US receives substantial quantities of precipitation arising from tropical and non-tropical sources throughout the growing season[5,13], accounting for early-season precipitation is critical to extract the signal of extreme events such as TCs. We regressed latewood width onto earlywood width[83–85] at the series level and calculated the adjusted latewood index (LWa) by adding 1 to the retained residuals to produce a time series with a mean of 1 (Supplementary Fig. 3)[33]. Although this approach is traditionally applied at the chronology level, calculating LWa at the series level allows us to further minimize the possible influence of non-climatic factors on individual series (e.g., microtopography)[33,41].

Data and climate screening. We collected seasonal (July 1–September 30) TCP data from the TCP Dataset (TCPDat)[5] for the grid point corresponding to the DNF in Mississippi (coordinates: 31.08, −89.08; Fig. 1a), summing the values for each 3-month season during the common period (1948–2012 CE). We defined seasonal TCP based on the period during which latewood growth and TCP predominantly coincide at the field site[5,31,86]. Given that TCs are but one source of precipitation in DNF, we also collected seasonal non-TCP and total precipitation (TCP + non-TCP) to determine the primary hydroclimatic contributor to latewood growth (Supplementary Figs. 1 and 4). Next, we examined the relationship between LWa and TCP at time lags 0 (t) and 1 ($t + 1$), only retaining records exhibiting a significant correlation. We correlated LWa with seasonal totals of TCP, non-TCP, and total precipitation at the grid point in TCPDat[5] corresponding to DNF (Fig. 2a, b and Supplementary Fig. 4). LWa consistently had stronger correlations with TCP ($r = 0.64$) than non-TCP ($r = 0.40$) and total precipitation ($r = 0.54$; Fig. 2a, b and Supplementary Fig. 4).

TCP reconstruction. To reconstruct TCP, we ran a linear regression of instrumental seasonal (July–September) TCP totals on our LWa chronology (Fig. 2a). We defined the calibration period as 1948 to 2012 based on the earliest year in TCPDat[5] and the most recent year with a minimum series sample depth of at least five (Supplementary Fig. 2). The chronology at $t + 1$ was not significant, and therefore, we assume that TCP and latewood production are annually coincident.

Split-sample calibration and validation are commonly used to examine whether the reconstruction is temporally stable (Supplementary Tables 1 and 2). This consists of dividing the common period (1948–2012 for this study) in half between an early period and a late period. Next, we verified our model by using one half (e.g., 1948–1980) to calibrate the model and predict TCP during the other half (e.g., 1981–2012). We did this for both halves of the common period as well as the full interval (1948–2012). In all stages of model verification, we calculated values for R^2, reduction of error statistic (RE)[87], and coefficient of efficiency (CE)[88] to assess prediction skill. Our RE and CE values are positive (Supplementary Tables 1 and 2), indicating that the predictive skill of our TCP reconstruction model remains stable through time. However, given the change in R^2 values between the split-sample periods, we also used a Bootstrapped Transfer Function Stability test (available in the R package dendRolAB) to examine the stability of the relationship during the calibration period[89]. Briefly, the Bootstrapped Transfer Function Stability test the null hypothesis as to whether the observed empirical cumulative distribution functions were obtainable given a perfectly stable relationship (parameter ratio = 1)[89]. If any of the parameters are <0.05, then the transfer function, and consequently, the relationship, is rejected as instable[89]. We resampled with replacement 1000 times throughout the calibration period (1948–2012 CE), using TCP and LWa as the predictand and predictor, respectively. In all cases, the p values of our parameters were greater than 0.05 (Supplementary Table 2), and we obtained positive bootstrapped RE (0.140) and CE (0.110) values. Finally, we autocorrelated TCP to determine whether TCP totals are independent of TCP totals for previous years (Supplementary Fig. 5) using the "autocorr" function in MATLAB. We determined the length of our record using the EPS and RBAR values at the cutoff date (EPS: 0.815; RBAR: 0.321).

Climate controls. To understand the full range of TCP variability, it is important to identify possible climatic controls. We collected indices representing different modes of climate variability that are known to exhibit any relationship to TCs, including genesis, tracks, or precipitation. A combination of indices from instruments and proxies were used to examine the connection between TCP and large-scale climate patterns. We looked at the relationship between TCP and indices of the AMV and the North Atlantic Subtropical High/Bermuda High (NASH/BH).

We examined the relationship between the NASH and reconstructed TCP during the common era using the BHI, which is the z-score representing the meridional pressure gradient between New Orleans, Louisiana, USA and Bermuda[42,90,91]. The BHI can be used to broadly assess positional or intensity variations in the western flank of the subtropical high. We focus on the BHI rather than indices of the North Atlantic Oscillation as the former is more representative of large-scale circulation in the North Atlantic during hurricane season[5,12,91–93]. Moreover, the NASH is an important driver of spatiotemporal variations in TCP throughout much of the Southeast US, including in DNF[5]. We seasonally weighted BHI values using monthly total TC landfall frequency to reduce the influence of the western flank outside of the peak in hurricane season (i.e., September) before correlating both time series using Spearman's rank correlation (Fig. 3a–c).

Previous studies have predominantly focused on using the Atlantic Multidecadal Oscillation to understand how TC behavior shifts with Atlantic Multidecadal Oscillation phases[15,94,95]. Given the uncertainty regarding the origins of the oscillatory behavior of the Atlantic Multidecadal Oscillation[57], we examined multidecadal connections between TCP and SSTs in the North Atlantic using a 1300-year AMV reconstruction published by Wang et al.[58] This reconstruction was developed by compiling North Atlantic SSTs reconstructions derived from multiple proxies across Europe and North America[58]. Using the sample cross-correlation function in MATLAB (crosscorr), we cross-correlated the AMV reconstruction with our TCP record using unfiltered and averaged (25- and 45-year moving windows based on multidecadal behavior in North Atlantic SSTs)[58] time series to examine whether TCP lagged or was concurrent with AMV (Fig. 4b and Supplementary Figs. 7 and 8B). We accounted for autocorrelation in both records by calculating new confidence intervals following the procedures described by Cryer and Chan[96] and Dean and Dunsmuir[97]. The new confidence intervals substantially increased the threshold needed to achieve significance. Additionally, we examined the effect of moving window length on the cross-correlation results, demonstrating that while moving averages can inflate the relationship, the correlation values equilibrate ($r = ~0.60$) at a window size of ~30+ years (Supplementary Fig. 6). Considering this, we also performed a cross wavelet transformation[98] using the xwt[99] function in MATLAB to examine potential relationships between the two long time series (Supplementary Fig. 10). In addition to showing the strength of the relationship, the xwt function also determines whether the two time series are in-phase (right-facing arrows in Supplementary Fig. 10), anti-phase (left-facing arrows), or offset by 90° with the AMV leading TCP (down-facing)[98,99].

We used a reconstruction of SST values from the north-northwest Gulf of Mexico to examine relationships between the Loop Current[100] and TCP. Reconstructed SST values were derived from isotopic ratios (i.e., $\delta^{18}O$ and Mg/Ca) of the planktic foraminifer *Globigerinoides ruber* as a proxy for the Loop Current[100], an extension of the AWP. Increases in SST are inferred to represent conditions during which the Loop Current is positioned farther into the Gulf of Mexico or undergoes a period of increased warm-core eddy shedding[100,101]. Compared to earlier reconstructions[101], the reconstruction from Thirumalai et al.[100] yields a higher resolution record of Loop Current activity during the late Holocene. However, the resolution was still too low to have a meaningful sample size for correlation. Nevertheless, given the known relationship between the Loop Current and TCs during the observational record, we used this reconstruction[100] to understand past multidecadal changes in the thermal characteristics of the Gulf of Mexico and provide additional context to long-term TCP variability along the north-central Gulf Coast (Fig. 4c, d).

Given that volcanic eruptions may act as an external forcing for SST variability in the North Atlantic[57–59], we decided to examine whether eruptions influenced TCP at our site. We performed a superposed epoch analysis using the R package dplR[102] to determine how annual TCP totals respond to volcanic eruptions (Fig. 3e). We selected eruption events[47,48] based on their likelihood of having a global or regional (i.e., Gulf of Mexico/Southeast US) climate impact (Supplementary Table 3). We included events located outside of North America if the eruption occurred in the Northern Hemisphere or equatorial latitudes and had a VEI ≥ 6 as these events affected global climate (e.g., Tambora in 1815). For volcanoes located in North America, we included events if the eruption occurred in tropical to subtropical latitudes, were not east of our site, and had a VEI ≥ 4. The lower explosivity threshold for North American volcanoes allowed us to consider regional climate variability due to changes in radiative forcing from volcanic ash[47].

Data availability
TCP Data (TCPDat)[5] is publicly available at https://github.com/jbregy/TCPDat. The TCP reconstruction from this paper is publicly available at the International Tree Ring Data Bank in the Paleoclimatology Data hosted by NOAA's National Centers for Environmental Information (https://www.ncei.noaa.gov/access/paleo-search/study/36470)[103]. Monthly MSLP reanalysis data for the BHI can be found at the Physical Sciences Laboratory at NOAA's National Centers for Environmental Prediction (https://downloads.psl.noaa.gov/Datasets/ncep.reanalysis.derived/surface/)[104]. The AMV reconstruction[58] can be found in the Paleoclimatology Data website hosted by NOAA's National Centers for Environmental Information (https://www.ncei.noaa.gov/access/paleo-search/study/22031)[105]. Data for the Mg/Ca-based SST reconstruction[100] can be found at NOAA's National Centers for Environmental Information (https://www.ncdc.noaa.gov/paleo-search/study/23373)[106]. Global summary of the month data shown in Supplementary Fig. 1 can be obtained from the Climate Data Online page at NOAA's National Centers for Environmental Information (https://www.ncdc.noaa.gov/cdo-web/)[107].

Code availability
Custom code used in this paper are available from the corresponding author upon request. Current and future versions of this code will be hosted at https://github.com/jbregy.

References

1. Rappaport, E. N. Fatalities in the United States from Atlantic Tropical Cyclones: new data and interpretation. *B. Am. Meteorol. Soc* **95**, 341–346 (2014).
2. Bessette-Kirton, E. K., Coe, J. A., Schulz, W. H., Cerovski-Darriau, C. & Einbund, M. M. Mobility characteristics of debris slides and flows triggered by Hurricane Maria in Puerto Rico. *Landslides* **17**, 2795–2809 (2020).
3. Paerl, H. W. et al. Recent increase in catastrophic tropical cyclone flooding in coastal North Carolina, USA: long-term observations suggest a regime shift. *Sci. Rep.* **9**, 10620 (2019).
4. Erickson, T. B., Brooks, J., Nilles, E. J., Pham, P. N. & Vinck, P. Environmental health effects attributed to toxic and infectious agents following hurricanes, cyclones, flash floods and major hydrometeorological events. *J. Toxicol. Env. Heal. B.* **22**, 157–171 (2019).
5. Bregy, J. C. et al. Spatiotemporal variability of tropical cyclone precipitation using a high-resolution, gridded (0.25° × 0.25°) dataset for the Eastern United States, 1948–2015. *J. Clim.* **33**, 1803–1819 (2020).
6. Vano, J. A. et al. Hydroclimatic extremes as challenges for the water management community: lessons from Oroville Dam and Hurricane Harvey. *B. Am. Meteorol. Soc* **100**, S9–S14 (2019).
7. Hein, C. J. et al. Shoreline dynamics along a developed River Mouth Barrier Island: multi-decadal cycles of erosion and event-driven mitigation. *Front. Earth Sci.* **7**, 1–23 (2019).
8. Maxwell, J. T., Ortegren, J. T., Knapp, P. A. & Soulé, P. T. Tropical cyclones and drought amelioration in the Gulf and Southeastern Coastal United States. *J. Clim.* **26**, 8440–8452 (2013).
9. Kossin, J. P. A global slowdown of tropical-cyclone translation speed. *Nature* **558**, 104–107 (2018).
10. Knutson, T. et al. Tropical cyclones and climate change assessment: part II: projected response to anthropogenic warming. *B. Am. Meteorol. Soc* **101**, E303–E322 (2020).
11. Knowles, J. T. & Leitner, M. Visual representations of the spatial relationship between Bermuda high strengths and Hurricane Tracks. *Cartogr. Perspect.* **56**, 37–51 (2007).
12. Li, L., Li, W. & Kushnir, Y. Variation of the North Atlantic subtropical high western ridge and its implication to southeastern US summer precipitation. *Clim. Dynam.* **39**, 1401–1412 (2012).
13. Labosier, C. F. & Quiring, S. M. Hydroclimatology of the Southeastern USA. *Clim. Res.* **57**, 157–171 (2013).
14. Aryal, Y. N., Villarini, G., Zhang, W. & Vecchi, G. A. Long term changes in flooding and heavy rainfall associated with North Atlantic tropical cyclones: roles of the North Atlantic Oscillation and El Niño–Southern Oscillation. *J. Hydrol.* **559**, 698–710 (2018).
15. Nogueira, R. C., Keim, B. D., Brown, D. P. & Robbins, K. D. Variability of rainfall from tropical cyclones in the eastern USA and its association to the AMO and ENSO. *Theor. Appl. Climatol.* **112**, 273–283 (2013).
16. Trenberth, K. E., Cheng, L., Jacobs, P., Zhang, Y. & Fasullo, J. Hurricane Harvey links to ocean heat content and climate change adaptation. *Earths Future* **6**, 730–744 (2018).
17. Knutson, T. et al. Tropical cyclones and climate change assessment: part I: detection and attribution. *B. Am. Meteorol. Soc* **100**, 1987–2007 (2019).
18. Landsea, C. W. & Franklin, J. L. Atlantic Hurricane database uncertainty and presentation of a new database format. *Mon. Weather Rev.* **141**, 3576–3592 (2013).
19. Wallace, D. J., Woodruff, J. D., Anderson, J. B. & Donnelly, J. P. Palaeohurricane reconstructions from sedimentary archives along the Gulf of Mexico, Caribbean Sea and western North Atlantic Ocean margins. *Geol. Soc. Spec. Publ.* **388**, 481–501 (2014).
20. Oliva, F., Viau, A. E., Peros, M. C. & Bouchard, M. Paleotempestology database for the western North Atlantic basin. *Holocene* **28**, 1664–1671 (2018).
21. Liu, K.-b & Fearn, M. L. Reconstruction of prehistoric landfall frequencies of catastrophic hurricanes in northwestern Florida from lake sediment records. *Quat. Res.* **54**, 238–245 (2000).
22. Brandon, C. M., Woodruff, J. D., Lane, D. P. & Donnelly, J. P. Tropical cyclone wind speed constraints from resultant storm surge deposition: a 2500 year reconstruction of hurricane activity from St. Marks, FL. *Geochem. Geophy. Geosy.* **14**, 2993–3008 (2013).
23. Bregy, J. C., Wallace, D. J., Minzoni, R. T. & Cruz, V. J. 2500-year paleotempestological record of intense storms for the northern Gulf of Mexico, United States. *Mar. Geol.* **396**, 26–42 (2018).
24. Wallace, E. J. et al. Intense Hurricane activity over the past 1500 years at South Andros Island, The Bahamas. *Paleoceanogr. Paleoclimatol.* **34**, 1761–1783 (2019).
25. Schmitt, D., Gischler, E., Anselmetti, F. S. & Vogel, H. Caribbean cyclone activity: an annually-resolved Common Era record. *Sci. Rep.* **10**, 1–17 (2020).
26. Winkler, T. S. et al. Revising evidence of hurricane strikes on Abaco Island (The Bahamas) over the last 680 years. *Sci. Rep.* **10**, 1–17 (2020).
27. Wallace, E. J. et al. 1050 years of hurricane strikes on Long Island in The Bahamas. *Paleoceanogr. Paleoclimatol.* **36**, 1–22 (2021).
28. Wallace, E. J., Dee, S. G. & Emanuel, K. A. Resolving long-term variations in North Atlantic tropical cyclone activity using a pseudo proxy paleotempestology network approach. *Paleoceanogr. Paleoclimatol.* **48**, 1–13 (2021).
29. Frappier, A. B. et al. Two millennia of tropical cyclone-induced mud layers in a northern Yucatán stalagmite: multiple overlapping climatic hazards during the Maya Terminal Classic "megadroughts". *Geophys. Res. Lett.* **41**, 5148–5157 (2014).
30. Miller, D. L. et al. Tree-ring isotope records of tropical cyclone activity. *Proc. Natl. Acad. Sci. USA* **103**, 14294–14297 (2006).
31. Knapp, P. A., Maxwell, J. T. & Soulé, P. T. Tropical cyclone rainfall variability in coastal North Carolina derived from longleaf pine (Pinus palustris Mill.): AD 1771–2014. *Clim. Change* **135**, 311–323 (2016).
32. Knapp, P. A., Soulé, P. T., Maxwell, J. T., Ortegren, J. T. & Mitchell, T. J. Tropical cyclone precipitation regimes since 1750 and the Great Suppression of 1843–1876 along coastal North Carolina, USA. *Int. J. Climatol.* **41**, 200–210 (2021).
33. Maxwell, J. T. et al. Recent increases in tropical cyclone precipitation extremes over the US East Coast. *Proc. Natl. Acad. Sci. USA* **118**, e2105636118 (2021).
34. Oswalt, C. & Guldin, J. M. Status of longleaf pine in the South: an FIA update. 25 p. Unpublished report. On file with: Chris Oswalt, Southern Research Station, Forest Inventory and Analysis, 4700 Old Kingston Pike, Knoxville, TN 37919. https://www.fs.usda.gov/treesearch/pubs/61790 (2021).
35. Herrmann, N. P. et al. Historical bioarchaeology and DVI: data integration of the Mississippi State Asylum burial sample and archival records. *Am. J. Phys. Anthropol.* **162**, 215–216 (2017).
36. Harley, G. L., Maxwell, J. T., Holt, D. & Speagle, C. B. Construction history of the Deason House, Jones County, Mississippi. *Dendrochronologia* **43**, 50–58 (2017).
37. Guzman, O. & Jiang, H. Global increase in tropical cyclone rain rate. *Nat. Commun.* **12**, 5344 (2021).
38. Foster, V. M. & McCutcheon, T. E. *Bulletin 44: Forrest County Mineral Resources* (ed. Mississippi State Geological Survey) 87 (University of Mississippi, 1941).
39. Brown, G. F. *Bulletin 58: Geology and Groundwater Resources of the Camp Shelby Area* (ed. Mississippi State Geological Survey) 72 (University of Mississippi, 1944).
40. United States Forest Service. *National Forests in Mississippi* (ed. U.S. Department of Agriculture) 210 (U.S. Forest Service, Region 8, 2014).
41. Montpellier, E. E., Knapp, P. A., Soulé, P. T. & Maxwell, J. T. Microelevational differences affect longleaf pine (Pinus palustris Mill.) sensitivity to tropical cyclone precipitation: a case study using LiDAR. *Tree-Ring Res.* **76**, 89–93 (2020).
42. Katz, R. W., Parlange, M. B. & Tebaldi, C. Stochastic modeling of the effects of large-scale circulation on daily weather in the Southeastern U.S. *Clim. Change* **60**, 189–216 (2003).
43. Colbert, A. J. & Soden, B. J. Climatological variations in North Atlantic tropical cyclone tracks. *J. Clim.* **25**, 657–673 (2012).
44. Evan, A. T. Atlantic hurricane activity following two major volcanic eruptions. *J. Geophys. Res. Atmos.* **117**, 1–8 (2012).
45. Guevara-Murua, A., Hendy, E. J., Rust, A. C. & Cashman, K. V. Consistent decrease in North Atlantic Tropical Cyclone frequency following major volcanic eruptions in the last three centuries. *Geophys. Res. Lett.* **42**, 9425–9432 (2015).
46. Yan, Q., Zhang, Z. & Wang, H. Divergent responses of tropical cyclone genesis factors to strong volcanic eruptions at different latitudes. *Clim. Dynam.* **50**, 2121–2136 (2017).
47. Altman, J. et al. Large volcanic eruptions reduce landfalling tropical cyclone activity: evidence from tree rings. *Sci. Total Environ.* **775**, 1–8 (2021).
48. Ammann, C. M. & Naveau, P. Statistical analysis of tropical explosive volcanism occurrences over the last 6 centuries. *Geophys. Res. Lett.* **30**, 1–4 (2003).
49. Tejedor, E., Steiger, N. J., Smerdon, J. E., Serrano-Notivoli, R. & Vuille, M. Global hydroclimatic response to tropical volcanic eruptions over the last millennium. *Proc. Natl. Acad. Sci. USA* **118**, 1–9 (2021).
50. Rao, M. P. et al. European and Mediterranean hydroclimate responses to tropical volcanic forcing over the last millennium. *Geophys. Res. Lett.* **44**, 5104–5112 (2017).
51. Gu, G. & Adler, R. F. Precipitation and temperature variations on the interannual time scale: assessing the impact of ENSO and volcanic eruptions. *J. Clim.* **24**, 2258–2270 (2011).
52. Cole-Dai, J. Volcanoes and climate. *WIRES Clim. Change* **1**, 824–839 (2010).

53. Bretl, S. et al. The influence of absorbed solar radiation by Saharan dust on hurricane genesis. *J. Geophys. Res. Atmos.* **120**, 1902–1917 (2015).
54. Hayes, C. T. & Wallace, D. J. Exploring records of Saharan dust transport and hurricanes in the western North Atlantic over the Holocene. *Quat. Sci. Rev.* **205**, 1–9 (2019).
55. Wielicki, B. A. et al. Evidence for large decadal variability in the tropical mean radiative energy budget. *Science* **295**, 841–844 (2002).
56. Evan, A. T., Foltz, G. R., Zhang, D. & Vimont, D. J. Influence of African dust on ocean–atmosphere variability in the tropical Atlantic. *Nat. Geosci.* **4**, 762–765 (2011).
57. Mann, M. E., Steinman, B. A., Brouillette, D. J. & Miller, S. K. Multidecadal climate oscillations during the past millennium driven by volcanic forcing. *Science* **371**, 1014–1019 (2021).
58. Wang, J. et al. Internal and external forcing of multidecadal Atlantic climate variability over the past 1,200 years. *Nat. Geosci.* **10**, 512–517 (2017).
59. Waite, A. J. et al. Observational and model evidence for an important role for volcanic forcing driving Atlantic multidecadal variability over the last 600 years. *Geophys. Res. Lett.* **47**, e2020GL089428 (2020).
60. Nigam, S. & Guan, B. Atlantic tropical cyclones in the twentieth century: natural variability and secular change in cyclone count. *Clim. Dyn.* **36**, 2279–2293 (2011).
61. Lin, Y., Zhao, M. & Zhang, M. Tropical cyclone rainfall area controlled by relative sea surface temperature. *Nat. Commun.* **6**, 6591 (2015).
62. Wang, C., Enfield, D. B., Lee, S.-K. & Landsea, C. W. Influences of the Atlantic Warm Pool on Western Hemisphere Summer Rainfall and Atlantic Hurricanes. *J. Clim.* **19**, 3011–3028 (2006).
63. Wang, C., Lee, S.-K. & Enfield, D. B. Atlantic Warm Pool acting as a link between Atlantic Multidecadal Oscillation and Atlantic tropical cyclone activity. *Geochem. Geophy. Geosyst.* **9**, 1–17 (2008).
64. Putrasahan, D. A., Kamenkovich, I., Le Hénaff, M. & Kirtman, B. P. Importance of ocean mesoscale variability for air-sea interactions in the Gulf of Mexico. *Geophys. Res. Lett.* **44**, 6352–6362 (2017).
65. Hakim, G. J. et al. The last millennium climate reanalysis project: Framework and first results. *J. Geophys. Res. Atmos.* **121**, 6745–6764 (2016).
66. Anderson, D. M. et al. Additions to the Last Millennium Reanalysis Multi-Proxy Database. *Data Sci. J.* **18** https://doi.org/10.5334/dsj-2019-002 (2019).
67. Tardif, R. et al. Last Millennium Reanalysis with an expanded proxy database and seasonal proxy modeling. *Clim. Past* **15**, 1251–1273 (2019).
68. Leland, C. et al. Dendroarcheological analysis of the Terminal Warehouse in New York City reveals a history of long-distance timber transport during the Gilded Age. *J. Archaeol. Res. Rep.* **39**, 103114 (2021).
69. Lombardi, R. et al. Fluvial activity in major river basins of the eastern United States during the Holocene. *Holocene* **30**, 1279–1295 (2020).
70. Muñoz, S. E. et al. Climatic control of Mississippi River flood hazard amplified by river engineering. *Nature* **556**, 95–98 (2018).
71. Stone, M. H. & Cohen, S. The influence of an extended Atlantic hurricane season on inland flooding potential in the southeastern United States. *Nat. Hazard. Earth Syst.* **17**, 439–447 (2017).
72. Mitchell, T. J., Knapp, P. A. & Patterson, T. W. The importance of infrequent, high-intensity rainfall events for longleaf pine (Pinus palustris Mill.) radial growth and implications for dendroclimatic research. *Trees Forests and People* **1**, 100009 (2020).
73. Pederson, N. External characteristics of old trees in the eastern deciduous forest. *Nat. Area. J.* **30**, 396–407 (2010).
74. Stokes, M. A. & Smiley, T. L. *An Introduction to Tree-Ring Dating* (The University of Chicago, Chicago Press, 1968).
75. Speer, J. H. *Fundamentals of Tree-Ring Research* 333 (University of Arizona Press, 2010).
76. Swetnam, T. W. Aged crossdating. *J. Forest.* **83**, 54–54 (1985).
77. Yamaguchi, D. K. A simple method for cross-dating increment cores from living trees. *Can. J. Forest. Res.* **21**, 414–416 (1991).
78. Holmes, R. L. *Program COFECHA User's Manual* (Laboratory of Tree-Ring Research, University of Arizona, 1983).
79. White, C. R. & Harley, G. L. Historical fire in longleaf pine (Pinus palustris) forests of south Mississippi and its relation to land use and climate. *Ecosphere* **7**, 1–17 (2016).
80. Cook, E. R. & Holmes, R. L. *User Manual for Program ARSTAN* (Laboratory of Tree-Ring Research, 1984).
81. Cook, E. R. & Peters, K. The smoothing spline: a new approach to standardizing forest interior tree-ring width series for dendroclimatic studies. *Tree-Ring Bull.* **41**, 45–53 (1981).
82. Bussberg, N. W., Maxwell, J. T., Robeson, S. M. & Huang, C. The effect of end-point adjustments on smoothing splines used for tree-ring standardization. *Dendrochronologia* **60**, 125665 (2020).
83. Meko, D. M. & Baisan, C. H. Pilot study of latewood-width of conifers as an indicator of variability of summer rainfall in the North American monsoon region. *Int. J. Climatol.* **21**, 697–708 (2001).
84. Stahle, D. W. et al. Cool- and warm-season precipitation reconstructions over western New Mexico. *J. Clim.* **22**, 3729–3750 (2009).

85. Griffin, D., Meko, D. M., Touchan, R., Leavitt, S. W. & Woodhouse, C. A. Latewood chronology development for summer-moisture reconstruction in the US Southwest. *Tree-Ring Res.* **67**, 87–101 (2011).
86. Kossin, J. P., Camargo, S. J. & Sitkowski, M. Climate modulation of North Atlantic hurricane tracks. *J. Clim.* **23**, 3057–3076 (2010).
87. Fritts, H. C. *Tree Rings and Climate* (Academic Press, 1976).
88. Nash, J. E. & Sutcliffe, J. V. River flow forecasting through conceptual models part I—a discussion of principles. *J. Hydrol.* **10**, 282–290 (1970).
89. Buras, A., Zang, C. & Menzel, A. Testing the stability of transfer functions. *Dendrochronologia* **42**, 56–62 (2017).
90. Stahle, D. W. & Cleaveland, M. K. Reconstruction and analysis of spring rainfall over the Southeastern U.S. for the past 1000 years. *B. Am. Meteorol. Soc.* **73**, 1947–1961 (1992).
91. Ortegren, J. T., Knapp, P. A., Maxwell, J. T., Tyminski, W. P. & Soulé, P. T. Ocean–atmosphere influences on low-frequency warm-season drought variability in the Gulf Coast and Southeastern United States. *J. Appl. Meteorol. Clim.* **50**, 1177–1186 (2011).
92. Davis, R. E., Hayden, B. P., Gay, D. A., Phillips, W. L. & Jones, G. V. The North Atlantic subtropical anticyclone. *J. Clim.* **10**, 728–744 (1997).
93. Li, W., Li, L., Fu, R., Deng, Y. & Wang, H. Changes to the North Atlantic subtropical high and its role in the intensification of summer rainfall variability in the southeastern United States. *J. Clim.* **24**, 1499–1506 (2011).
94. Hetzinger, S. et al. Caribbean coral tracks Atlantic Multidecadal Oscillation and past hurricane activity. *Geology* **36**, 11–14 (2008).
95. Klotzbach, P. J. The influence of El Niño–Southern Oscillation and the Atlantic Multidecadal Oscillation of Caribbean tropical cyclone activity. *J. Clim* **24**, 721–731 (2011).
96. Cryer, J. D. & Chan, K.-S. *Time Series Analysis: With Application in R* 2nd edn (Springer-Verlag, 2008).
97. Dean, R. T. & Dunsmuir, W. T. Dangers and uses of cross-correlation in analyzing time series in perception, performance, movement, and neuroscience: the importance of constructing transfer function autoregressive models. *Behav. Res. Methods* **48**, 783–802 (2016).
98. Grinsted, A., Moore, J. C. & Jevrejeva, S. Application of the cross wavelet transform and wavelet coherence to geophysical time series. *Nonlin. Processes Geophys.* **11**, 561–566 (2004).
99. Grinsted, A. Cross wavelet and wavelet coherence v. 1.0.0.0 (MATLAB, 2017).
100. Thirumalai, K. et al. Pronounced centennial-scale Atlantic Ocean climate variability correlated with Western Hemisphere hydroclimate. *Nat. Commun.* **9**, 1–11 (2018).
101. Richey, J. N., Poore, R. Z., Flower, B. P. & Quinn, T. M. 1400 yr multiproxy record of climate variability from the northern Gulf of Mexico. *Geology* **35**, 423–426 (2007).
102. Bunn, A. G. A dendrochronology program library in R (dplR). *Dendrochronologia* **26**, 115–124 (2008).
103. Bregy, J. C. et al. De Soto National Forest, Mississippi tropical cyclone precipitation reconstruction from 1540–2012 CE. https://www.ncei.noaa.gov/access/paleo-search/study/36470 (2022).
104. Physical Sciences Laboratory, National Centers for Environmental Prediction, National Oceanic and Atmospheric Administration. NCEP reanalysis derived surface. https://downloads.psl.noaa.gov/Datasets/ncep.reanalysis.derived/surface/ (1996).
105. Wang, J. L. et al. 1200 year Atlantic multidecadal variability and Atlantic Multidecadal Oscillation reconstructions. https://www.ncei.noaa.gov/access/paleo-search/study/22031 (2017).
106. Thirumalai, K. et al. Garrison Basin, Gulf of Mexico d18O and Mg/Ca in three multicores, and stacked SST/d18Osw/SSS reconstructions spanning the past 4.4 kyrs. https://www.ncdc.noaa.gov/paleo-search/study/23373 (2018).
107. Climate Data Online, National Centers for Environmental Information, National Oceanic and Atmospheric Administration. https://www.ncdc.noaa.gov/cdo-web/ (2022).

Author contributions
J.C.B. processed and measured samples, collected instrumental TCP data, analyzed data, wrote the manuscript, and designed original figures using MATLAB, R, ArcGIS, and Adobe Illustrator. J.T.M. collected, processed, and measured samples, analyzed data, provided substantial input on the manuscript and figures, and designed original figures in R. G.L.H. collected, processed, and measured samples, analyzed data, provided

substantial input on the manuscript and figures, and designed original figures in ArcGIS and Adobe Illustrator. S.M.R. analyzed data, provided substantial input on the manuscript and figures, and designed original figures in MATLAB. E.A.E. analyzed data, provided substantial input on the manuscript and figures, and created original figures in Adobe Illustrator. K.J.H. analyzed data, provided substantial input on the manuscript and figures, and designed original figures by hand and in Adobe Illustrator.

Competing interests
The authors declare no competing interests.

Additional information
Supplementary information The online version contains supplementary material available at https://doi.org/10.1038/s43247-022-00494-7.

Correspondence and requests for materials should be addressed to Joshua C. Bregy.

Peer review information *Communications Earth & Environment* thanks the anonymous reviewers for their contribution to the peer review of this work. Primary Handling Editors: Adam Switzer, Joe Aslin. Peer reviewer reports are available.

Reprints and permission information is available at http://www.nature.com/reprints

Publisher's note Springer Nature remains neutral with regard to jurisdictional claims in published maps and institutional affiliations.